OXFORD CENTRE FOR COLLABORATIVE APPLIED MATHEMATICS

Report Number 10/06

Derivation of a dual porosity model for the uptake of nutrients by root hairs

by

Konstantinos C. Zygalakis and Tiina Roose

Oxford Centre for Collaborative Applied Mathematics
Mathematical Institute
24 - 29 St Giles'
Oxford
OX1 3LB
England

Bulletin of Mathematical Biology manuscript No.
(will be inserted by the editor)

Derivation of a dual porosity model for the uptake of nutrients by root hairs

Konstantinos C. Zygalakis[1] **and Tiina Roose**[1,2]

[1] Oxford Centre for Collaborative Applied Mathematics, University of Oxford, 24 - 29 St Giles' Oxford OX1 3LB.
[2] School of Mathematics, University of Southampton, University Road, Southampton SO17 1BJ

The date of receipt and acceptance will be inserted by the editor

Abstract Root hairs are thought to play an important role in mediating nutrient uptake by plants. We develop a mathematical model for the nutrient transport and uptake in the root hair zone of a single root in the soil. Nutrients are assumed to diffuse both in the soil fluid phase and within the soil particles. Nutrients can also be bound to the soil particle surfaces by reversible reactions. Using homogenization techniques we derive a macroscopic dual porosity model for nutrient diffusion and reaction in the soil which includes the effect of all root hair surfaces.

Key words Homogenization, dual porosity, nutrient uptake, root hairs, phosphate.

1 Introduction

With the recent reports in global food shortages it is now more important than ever to have a clear understanding of processes that control crop growth [1]. One of the most influential factors for plant growth is the soil nutrient status and the availability of the nutrients in the soil solution. Plants are able to take up nutrients from the soil solution using their root system. An integral part of the root system is root hairs, which are lateral extensions of epidermical cells that increase the effective surface area of the root system available for water and nutrient uptake. Nutrients move to the root and the root hairs by a combination of diffusion and convection in the soil pore space [2].

One of the most limited nutrients, particularly in Africa, is phosphate which is usually so strongly bound to the soil particles as to become almost immobile [2]. In these situations of phosphate bioavailability, root hairs are

thought to be particularly important [3]. A better understanding of how root hairs mediate phosphate uptake will enhance the development of more phosphate-efficient crops, in addition to explaining how their morphology influences their function. Such an improved understanding might lead to the reduction in the use of phosphate based fertilizers. This would be welcoming for the developing world, since due to the lack of free phosphorous in nature, phosphate based fertilizes are becoming limited and expensive [1]. Futhermore, such a reduction would have a positive environmental impact, given that phosphate based fertilizers are posing a great environmental threat, especially in the developed world [4,5]. Given the complexity of root hair-soil interactions, and the difficulty of measuring the root uptake properties experimentally, development of mathematical models is necessary. Mathematical models will enable the comparisons between different root hair properties, such as their geometry and rates of nutrient uptake as well as different soil properties.

The more traditional approaches of root hair uptake modelling fall into three categories. In the first, the effective root radius is extended by the length of the root hairs, and any concentration gradients along the length of the root hair are not allowed [6]. In the second, the continuity equation for nutrient transport is modified with a separate sink term describing nutrient influx into the hairs [7]. Finally a more computationally intensive approach has been adopted in [8]. In particular, the nutrient transport equation is solved in a three-dimensional model that takes into account the geometry of root hairs explicitly. However, in all these models the soil around each root hair is considered homogeneous, *i.e.,* it is averaged over many soil particles. This assumption, as we later show, is not necessarily valid in all experimental situations.

The modelling of such multiscale problems in three-dimensions is computationally challenging and limited to the specific geometry under investigation. One possible way of overcoming such barriers is by using the homogenization theory [9,10]. With this method, spatial heterogeneities at different scales can be transformed into a tractable homogeneous description. Equations that are valid on the macroscale are derived by incorporating the relevant information about the microscale geometry and model properties.

Recently there has been an increase in the use of homogenization methods in studying nutrient transport in the rhizosphere [11–13]. More precisely, in [11] a model for the nutrient uptake by the root hairs was developed, where the effect of the root hairs was replaced, in the homogenized equation, by a sink term valid throughout the root hair zone. This model was applicable mainly in the case of hydroponic cultures and soils where the soil particle size is much smaller than the interhair distance. On the other hand, in [12,13] a dual porosity model was developed and studied for the diffusion of strongly-sorbed solutes, such as phosphate, in the soil. In this paper the nutrients were allowed to diffuse both in the soil solution and inside the soil particles, while reactions on the soil particles surfaces and in their interior surfaces were also taken into account.

In this paper we study the nutrient uptake by root hairs, in a single root scale as in [11], but not in hydroponic cultures. Instead, we consider the situation where the nutrients are allowed to diffuse and react in the solution and also within the soil particles as in [13]. The fact that the soil particle size is comparable to the interhair distance means that when we homogenize this system we should take into account both the effect of the root hairs and the soil particles simultaneously. As we show later this leads to an effective model that takes into account both the root hairs and soil particle geometry on the diffusion impedance.

The rest of the paper is organized as follows. In Section 2, we describe the microscopic model. In Section 3 we present the homogenized equations in the general case as well as a simplified one dimensional version of them. Finally, in Section 4 we present various numerical investigations of the homogenized equations.

2 Description of the model

In this section we describe our microscopic model. We start by describing the geometry of the simplest geometric element in the model and then present the dimensional and dimensionless forms of our equations. In order to describe the geometry of our model, we first need to discuss the relative size of the root hairs in comparison to the soil particles. A picture of root

Fig. 1: Root hairs of barley (source: wheat.pw.usda.gov/ggpages/bgn/34/KE.htm).

hairs in the case of barley can be seen in Figure 1. In Table 1 we present the interhair distance of root hairs for a variety of plants. As we can see the typical interhair distance is of the order of 10^{-2} cm. Since, the size of a typical soil particle is of the same order (for example sand particles can be of the order 10^{-2} cm [2,14]) we see that in between two root hairs we typically have one soil particle.

Plants	Root hair radius 10^{-4} cm	Interhair distance 10^{-2} cm
Arabidopsis	$3.2 - 3.3$	$0.92 - 1.11$
Bean	5	1.36
Carrot	4	0.61
Lettuce	4.8	0.78
Onion	1	4.27
Rape	5	1.02
Tomato	5	1.02
Wheat	5	$1.11 - 1.49$

Table 1: Root hair radius and interhair distance for different plants (see [11] and the references within).

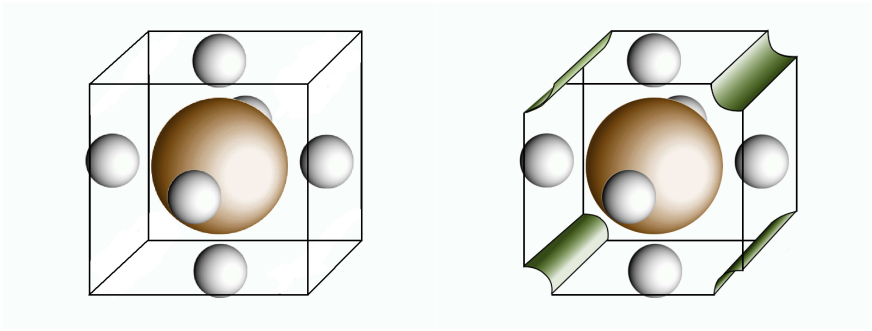

(a) Away from the root hair zone (b) In the root hair zone

Fig. 2: Typical geometry of the problem. Root hair surfaces are denoted with green, the soil particle with brown, while the gas particles with white. Rest is water

2.1 Geometry of the model

We consider one single root with a root hair zone in the soil. Soil is considered to be a porous material consisting of porous soil particles that are separated by water and air, see Figure 2a. A continuous film of liquid is in contact with and connects the particles. Figure 2a shows the typical geometry of the soil away from the root hair zone, while in the root hair zone the typical geometry can be seen in Figure 2b

The unit cell that we see in Figure 2 is periodically repeating itself in space. We therefore have a composite material with microscopic properties that change periodically and rapidly compared to the macroscopic scale. We define the macroscopic space variable $\mathbf{x}$ and the microscopic space variable $\mathbf{y}$. The characteristic macroscopic length scale is the length of the soil column $L = L_a + L_b$, where L_a is the length of the part of the soil column that is in the root hair zone and L_b is the length of the soil column away from the root hair zone. The characteristic microscopic length-scale is the length

l_1 of the inter-hair distance, which we assume to be of comparable size to the length l of the unit cell containing a single soil particle and its associated extra-particle liquid and gas. Based on the discussion in this section, we expect that there would be at most one or two particles within two root hairs.

If the ratio of the two length scales is small, *i.e.,* scaling parameter $\epsilon = l_1/L \ll 1$, it is possible to use homogenization theory to find effective macroscopic properties. Homogenization theory [9,10] enables us to develop equations allowing for the influence of both spatial coordinates: the $\mathbf{y}$ coordinates reflecting the microscopic properties of the system, and the coarser $\mathbf{x}$ coordinates reflecting the macroscopic properties. Homogenization theory considers that $\mathbf{x}$ and $\mathbf{y}$ can be treated independently if ϵ is sufficiently small.

We now proceed with first defining the dimensional equations for our model. We then non-dimensionalize these using the scale of the microscopic space. We later rescale them to obtain equations on the scale of the soil bulk and then apply homogenization theory to obtain a macroscopic equation.

2.2 Dimensional model

We will distinguish between the solute concentration in water between soil particles (interparticle water volume) C_e, $\mu mol\ cm^{-3}$ and in water inside each particle (intraparticle water volume) C_i $\mu mol\ cm^{-3}$. We take θ_i to be particle porosity, *i.e.,* the volume of water inside the particle per volume of particle and thus $\theta_i C_i$ $\mu mol\ cm^{-3}$ is the amount of solute in the water fraction of the particle per volume of the particle.

We also allow for adsorption and desorption of solutes to the soil particle surfaces. In the case of strongly sorbed solutes, such as phosphate, the adsorption and the desorption can be fast in comparison to diffusion. Thus, following [15] we consider fast and slow adsorbed solute concentration and will distinguish between adsorption to the surface of the particle and to the surfaces inside the porous particle. We thus define the following quantities: S_{ef} and S_{es}, $\mu mol\ cm^{-2}$, are fast and slow adsorbed concentrations on the single particle surface, respectively, and similarly S_{if} and S_{is}, $\mu mol\ cm^{-2}$ are fast and slow concentrations on the surfaces inside the single particle, respectively.

The solute concentration in the water in the interparticle space is changing due to diffusion in water, fast and slow adsorption and desorption on the particle surface and due to the flux into the particle. We point out that we ignore convective effects because the Peclet number for flows into the root is very small [16]. Thus the equations and boundary conditions for the solute concentration in water around the particle are given by

$$\partial_t C_e - \nabla \cdot (D_l \nabla C_e) = 0, \qquad \text{in solution around particles,} \quad (2.1a)$$

$$D_l \nabla C_e \cdot \nu = D_i \nabla C_i \cdot \nu - \partial_t(\sigma_e S_{ef}) - \partial_t(\sigma_e S_{es}), \quad (2.1b)$$

$$C_e = C_i, \qquad \text{on particle surface,} \quad (2.1c)$$

where D_e is the diffusion coefficient of solute in water, D_i is the diffusion coefficient of solute inside the particle and ν is the outward normal vector to the particle boundary (pointing into the particle). Also here σ_e, $cm^2 cm^{-2}$, defines the bulk density on the exterior particle surface per whole surface area of the particle and $\sigma_e S_{ef}$ and $\sigma_e S_{es}$, $\mu mol\ cm^{-2}$, are amounts of fast and slow absorbed solute per particle surface.

For the fast and slow adsorbed concentrations on the particle surface we take

$$\partial_t(\sigma_e S_{ef}) = \sigma_e F_f(C_e, S_{ef}), \quad \text{on particle surface,} \tag{2.2a}$$
$$\partial_t(\sigma_e S_{es}) = \sigma_e F_s(C_e, S_{es}), \quad \text{on particle surface,} \tag{2.2b}$$

where F_f and F_s are reaction kinetics for fast and slow adsorbed solute concentration on the particle surface, respectively. We will specify the function form of F_f and F_s at a later stage.

The solute concentration in the water fraction inside the particle is changing due to diffusion, adsorption and desorption on the solid surface inside the particle, and the flux of the solute concentration from interparticle to intraparticle domain. We thus obtain

$$\theta_i \partial_t C_i - \nabla \cdot (D_i \nabla C_i) = -\partial_t(\sigma_i S_{if}) - \partial_t(\sigma_i S_{is}), \text{ inside the particle,} \tag{2.3}$$

where the adsorbed concentration inside the particle is given by

$$\partial_t(\sigma_i S_{if}) = \sigma_i G_f(C_i, S_{if}), \quad \text{on particle surface,} \tag{2.4a}$$
$$\partial_t(\sigma_i S_{is}) = \sigma_i G_s(C_i, S_{is}). \quad \text{on particle surface.} \tag{2.4b}$$

In (2.4) G_f, G_s are reaction kinetics for fast and slow adsorbed solute concentrations inside the particle. We denote by σ_i, $cm^2\ cm^{-3}$, the bulk density in the interior particle surfaces per whole volume of the particle, and $\sigma_i S_{if}, \sigma_i S_{is}$, are amounts of fast and slow absorbed solute inside the particle per particle volume, respectively. For simplicity we only treat the case of linear kinetics:

$$F_j(C_e, S_{ej}) = \gamma_{aj} C_e - \gamma_{dj} S_{ej},$$
$$G_j(C_i, S_{ij}) = \zeta_{aj} C_i - \zeta_{dj} S_{ij}, \text{ for } j = f \text{ and } j = s.$$

We choose here a linear form for the reaction kinetics to simplify our calculations. The case of nonlinear kinetics in the absence of the root hairs has been treated rigorously, via the means of two scale convergence, in [13], where it was shown that the corresponding effective equation is valid for any sublinear reaction kinetics. The inclusion of root hairs in our formulation does not change the two-scale convergence results of [13], as long as the nutrient uptake by root hairs is sublinear.

2.2.1 Boundary conditions We now have to take into account the effect of the root hairs and the root itself. The nutrient uptake by the root hairs is described by the uptake function f_1, *i.e.,*

$$-D_l \nabla C_e \cdot \mathbf{n_h} = f_1, \text{ on } \partial\Omega_h. \tag{2.5}$$

The nutrient uptake by the root is described by the uptake function f_2, *i.e.,*

$$-D_l \nabla C_e \cdot \mathbf{n_r} = f_2, \text{ on } \partial\Omega_r, \tag{2.6}$$

where $\mathbf{n_h}, \mathbf{n_r}$ are the unit normals to the root hair surfaces and the root Ω_r, Ω_h respectively. The uptake functions f_1, f_2 represent Michaelis-Menten kinetics:

$$f_1 = \frac{F_h C_e}{K_h + C_e} - E_h, \tag{2.7a}$$

$$f_2 = \frac{F_r C_e}{K_r + C_e} - E_r, \tag{2.7b}$$

and the terms E_h, E_r represent the fact that after a minimum concentration in the soil pore fluid, pore fluid root and root hair uptake stops. These are the most popular functional forms for these functions in the plant literature [2], and since they are sublinear results of [13] hold.

2.3 Non-Dimensional model

We non-dimensionalize the equations in order to be able to apply the homogenization procedure. We set $t = [t]t^*, \mathbf{y} = [y]\mathbf{y}*, C_e = [C_e]C_e^*, C_i = [C_i]C_i^*, S_{ef} = [S_{ef}]S_{ef}^*, S_{if} = [S_{if}]S_{if}^*$, and $S_{is} = [S_{is}]S_{is}^*$. We will now discuss the choice of scales. In a representative experiment [15], the length of the domain containing a particle with radius $\rho = 4.49\ 10^{-3}$ cm surrounded by solution and air is $l_1 = 10^{-2}$ cm, which is of similar size to the interhair distance l [11], while the distance between neighbouring roots is $L = 1$ cm. For the purposes of our analysis from now on we will consider that the interhair distance l_1 is equal to the length of the domain containing a particle l. The typical length of the root hair zone $L_a = 10^{-1}$ cm [11].

In order to choose the appropriate timescale of diffusion, we need to take into account that we are interested in processes on the time scale of the whole domain. We thus choose a timescale of diffusion that takes place on soil sample scale $[t] = \frac{L^2}{D_l}$. In addition to the soil sample scale we also have a scale associated with the simplest element of the system, the soil particle [1]. Thus in order to see the influence of the diffusion inside the particle on the behaviour of the whole system we choose the length of the single particle domain (interhair distance) $[x] = l$, as scale for space. Due to the

[1] In principle we have one more characteristic length scale coming from the interhair distance, but we ignore it, since we have shown in Section 2.1 that it is of the same order with the particle size.

continuity condition $C_e = C_i$ on the surface of the particle, it is convenient to choose the scaling for concentrations to be the same, *i.e,* $[C_e] = [C_i]$. Also in the equations for C_e, C_i we have the concentrations of the adsorbed solute and thus for simplicity we choose the scales for the adsorbed solute to be proportional to $[C_e]$. Considering the differences in the dimensions we choose $[S_{ef}] = [S_{es}] = [C_e][x]/\sigma_e$ and $[S_{if}] = [S_{is}] = [C_i]/\sigma_i$. As a representative concentration we choose $[C_e] = K_h = 2.3 \times 10^{-3}$ μmol cm^{-3}, as was done in [18]. Note that K_h is the concentration when the root hair uptake is half of the maximum possible.

The value of the dimensionless parameter ϵ is 10^{-2}, which is equal to the ratio of length of a single particle domain l to the length of the soil domain L. We also define $r_0 = \rho/l$, *i.e.,* the ratio of the particle radius to the length of a single particle domain. Thus with the scales specified above, the dimensionless equations are given by

$$\partial_{t^*} C_e^* - \frac{1}{\epsilon^2}\nabla_y^2 C_e^* = 0, \quad \text{in interparticle space,} \tag{2.8a}$$

$$\nabla_y C_e^* \cdot \nu = \frac{D_i}{D_l}\nabla_y C_i^* \nabla \nu - \epsilon^2(\partial_{t^*} S_{ef}^* - \partial_{t^*} S_{es}^*), \quad \text{on particle surfaces,} \tag{2.8b}$$

$$C_e^* = C_i^*, \quad \text{on particle surfaces,} \tag{2.8c}$$

$$\partial_{t^*} S_{ef}^* = \bar{\gamma}_{af} C_e^* - \bar{\gamma}_{df} S_{ef}^*, \quad \text{on particle surfaces,} \tag{2.8d}$$

$$\partial_{t^*} S_{es}^* = \bar{\gamma}_{as} C_e^* - \bar{\gamma}_{ds} S_{es}^*, \quad \text{on particle surfaces,} \tag{2.8e}$$

$$\theta_i \partial_{t^*} C_i - \frac{D_i}{D_l \epsilon^2}\nabla_y^2 C_i = \partial_{t^*} S_{if}^* - \partial_{t^*} S_{is}^* \quad \text{inside particles,} \tag{2.8f}$$

$$\partial_{t^*} S_{if}^* = \bar{\zeta}_{af} C_i^* - \bar{\zeta}_{df} S_{if}^*, \quad \text{inside particles,} \tag{2.8g}$$

$$\partial_{t^*} S_{is}^* = \bar{\zeta}_{as} C_i^* - \bar{\zeta}_{ds} S_{is}^*, \quad \text{inside particles,} \tag{2.8h}$$

$$\nabla_y C_e^* \cdot \nu = 0, \quad \text{on surface of air domains,} \tag{2.8i}$$

$$-\nabla_y C_e^* \cdot \nu_h = \epsilon^2 F_1, \quad \text{on the root hairs surfaces,} \tag{2.8j}$$

$$-\nabla_y C_e^* \cdot \nu_r = \epsilon F_2, \quad \text{on the root surface,} \tag{2.8k}$$

where

$$\bar{\gamma}_{aj} = \gamma_{aj}\sigma_e \frac{L^2}{l D_l},$$
$$\bar{\gamma}_{dj} = \gamma_{dj}\frac{L^2}{D_l},$$
$$\bar{\zeta}_{aj} = \zeta_{aj}\sigma_i \frac{L^2}{D_l},$$
$$\bar{\zeta}_{dj} = \zeta_{dj}\frac{L^2}{D_l}, \text{ for } j = f \text{ and } j = s,$$

and F_1 is derived from (2.7) and it is given by

$$F_1 = \frac{\lambda_1 C_e}{1 + C_e} - \delta_1, \tag{2.9a}$$

$$\lambda_1 = \frac{L^2}{l D_l K_h} F_h, \tag{2.9b}$$

$$\delta_1 = \frac{L^2}{l D_l K_h} E_h. \tag{2.9c}$$

Similarly F_2 is given by

$$F_2 = \frac{\lambda_2 C_e}{\kappa_2 + C_e} - \delta_2, \tag{2.10a}$$

$$\kappa_2 = \frac{K_r}{K_h}, \tag{2.10b}$$

$$\lambda_2 = \frac{L}{D_l K_r} F_r, \tag{2.10c}$$

$$\delta_2 = \frac{L}{D_l K_r} E_r. \tag{2.10d}$$

The diffusion inside the particle D_i is much smaller than the diffusion in the free fluid part D_l. The typical relation $\frac{D_i}{D_l} \sim 10^{-4}$ is comparable to ϵ^2. Thus $\frac{D_i}{D_l \epsilon^2} \sim \mathcal{O}(1)$ in equation (2.8) and this is exactly the limit for which dual porosity effects become important.

We should also note the difference in the powers of ϵ in the scaling of boundary conditions. In particular, in (2.8j) we have scaled the boundary condition for the root hairs with ϵ^2, while in (2.8k) we have scaled the boundary condition for the main root with ϵ. This is the distinguished limit in which the model we obtain by homogenization is the most inclusive one. In particular, in this case, the effective equation obtained in the root hair zone contains a sink term related to the root hairs uptake. If however, for the given parameter values the root hair contribution is too weak ($F_1 < \mathcal{O}(1)$) or too strong ($F_1 > \mathcal{O}(1)$), then the effective model in the root hair zone would simplify as in [11] for the root hair uptake in hydroponics.

3 Homogenized model

Having set the conditions for coupling the micro and macro scales, we can rescale Equations (2.8) from the unit cell to the whole soil and obtain the homogenized macro-scale model. The formal derivation of these equations can be found in Appendix A. We divide our domain in two; the first being the root hair zone and the second being away from the root hair zone. Between these two domains we have continuity of fluxes and concentrations for C_e.

3.1 Homogenized equation in the root hair zone

The homogenized equation in the root hair zone is given by

$$\theta_a \frac{\partial C_e}{\partial t} = \nabla_x \cdot (D^a_{eff} \nabla_x C_e) + \frac{1}{|Z|} \int_{\partial Y_a} \hat{D} \nabla_y C_i \cdot \nu dS \tag{3.1a}$$
$$- \frac{1}{|Z|} \int_{\partial \Gamma} f_0 dS - \frac{1}{|Z|} \int_{\partial Y_a} \left(\frac{\partial S_{ef}}{\partial t} + \frac{\partial S_{es}}{\partial t} \right) dS,$$
$$\theta_i \frac{\partial C_i}{\partial t} = \hat{D} \nabla_y^2 C_i - \frac{\partial S_{if}}{\partial t} - \frac{\partial S_{is}}{\partial t}, \tag{3.1b}$$
$$C_e = C_i, \tag{3.1c}$$

where $\hat{D} = D_i/(D_l \epsilon^2) \sim \mathcal{O}(1)$ and $\theta_a = |X_a|/|Z|$. The different domains of integration are explained in Table 2. The effective diffusivity matrix D^a_{eff}

Domain	Meaning
Y_a	The volume covered by the soil particles in the unit cell.
∂Y_a	The boundary of the soil particles.
$\bar{Y}_a$	The air volume.
$\partial \bar{Y}_a$	The boundary of the air water interface.
Γ	The area covered by the root hairs.
$\partial \Gamma$	The boundary of the root hairs.
$X_a = (Z_a \setminus (Y_a \cup \bar{Y}_a) \cup \Gamma)$	The extraparticle fluid volume.

Table 2: Subdomains for the cell problem in the root hair zone.

is given by

$$D^a_{eff} = \frac{1}{|Z|} \int_{X_a} ((\nabla_y \chi)^T + I) dy.$$

The function χ is the solution of the cell problem

$$\nabla_y \cdot \nabla_y \chi = 0, \text{ on } X_a, \tag{3.2a}$$
$$(\nabla_y \chi + I) \cdot \nu = 0, \text{ on } \partial Y_a \cup \partial \bar{Y}_a \cup \partial \Gamma, \tag{3.2b}$$

where χ is periodic in Z_a. It is important to note that in (3.2) the impedance in the diffusion takes into account not only the soil particle (∂Y_a) and the air volume ($\partial \bar{Y}_a$), but also the existence of root hairs ($\partial \Gamma$).

3.2 Homogenized equation away from the root hair zone

The homogenized equation away from the root hair zone is given by

$$\theta_b \frac{\partial C_e}{\partial t} = \nabla_x \cdot (D^b_{eff} \nabla_x C_e) + \frac{1}{|Z|} \int_{\partial Y_b} \hat{D} \nabla_y C_i \cdot \nu dS \tag{3.3a}$$
$$- \frac{1}{|Z|} \int_{\partial Y_b} \left(\frac{\partial S_{es}}{\partial t} + \frac{\partial S_{ef}}{\partial t} \right) dS,$$
$$\theta_i \frac{\partial C_i}{\partial t} = \hat{D} \nabla_y^2 C_i - \frac{\partial S_{if}}{\partial t} - \frac{\partial S_{is}}{\partial t}, \tag{3.3b}$$
$$C_e = C_i, \tag{3.3c}$$

where $\hat{D} = D_i/(D_l \epsilon^2)$ and $\theta_a = |X_b|/|Z|$. Note that this is the same effective equation that has been derived in [13] using two scale convergence, and in [12] using homogenization. The different domains of integration are explained in Table 3. The effective diffusivity matrix D^b_{eff} is given by

Domain	Meaning
Y_b	The volume covered by the soil particles in the unit cell Z_b.
∂Y_b	The boundary of the soil particles .
$\bar{Y}_b$	The air volume.
$\partial \bar{Y}_b$	The boundary of the air water interface.
$X_b = (Z_b \setminus (Y_b \cup \bar{Y}_b))$	The extra particle fluid volume.

Table 3: Subdomains for the cell problem away from the root hair zone.

$$D^b_{eff} = \frac{1}{|Z|} \int_{X_b} ((\nabla_y \chi)^T + I) dy,$$

where χ is the solution of the cell problem

$$\nabla_y \cdot \nabla_y \chi = 0, \text{ on } X_b, \tag{3.4a}$$
$$(\nabla_y \chi + I) \cdot \nu = 0, \text{ on } \partial Y_b \cup \partial \bar{Y}_b, \tag{3.4b}$$

where χ is periodic in Z_b.

3.3 Simplification of the model

In this subsection we present various assumptions that allow us to reduce the model from three microstructure dimensions to one. More precisely, under the assumption $\bar{\gamma}_{df}, \bar{\zeta}_{df} = \frac{1}{\delta} \gg 1$, *i.e.,* desorption in the fast reaction is very fast in comparison to the diffusion we have that:

$$\delta \partial_t S_{ef} = \frac{\bar{\gamma}_{af}}{\bar{\gamma}_{df}} C_e - S_{ef}, \ \delta \partial_t S_{if} = \frac{\bar{\zeta}_{af}}{\bar{\zeta}_{df}} C_i - S_{if}.$$

This implies that the fast reactions can be assumed to be in equilibrium and

$$S_{ef} = \frac{\bar{\gamma}_{af}}{\bar{\gamma}_{df}} C_e, \quad S_{if} = \frac{\bar{\zeta}_{af}}{\bar{\zeta}_{df}} C_i,$$

and thus

$$\partial_t S_{ef} = \frac{\sigma_e \gamma_{af}}{l \gamma_{df}} \partial_t C_e, \ \partial_t S_{if} = \frac{\sigma_i \zeta_{af}}{\zeta_{df}} \partial_t C_i.$$

We will refer to the ratio $\frac{\bar{\gamma}_{af}}{\bar{\gamma}_{df}}$ as the soil buffer power [2].

Because particles are spherical we can consider diffusion only in the radial dimension. Therefore we can reduce the general model to a set of one-dimensional equations coupled via boundary conditions on the particle surface (Figure 3).

We consider a soil column of dimensionless length $x_1 = 1$, divided into two parts where the first contains the root hair zone and has dimensionless length $L_a/L = l_h$ and particles of radius $r = \rho$, where r is the radial coordinate within the particle (r varies from 0 to r_0). Thereby we obtain:

$$\begin{aligned}
\left(\theta_a + \frac{|\partial Y|}{|Z|}\frac{\sigma_e}{l}\frac{\gamma_{af}}{\gamma_{df}}\right)\partial_t C_e &= D^a_{eff}\partial_x^2 C_e - \hat{D}\frac{|\partial Y|}{|Z|}\partial_r C_i(t,x,r)\Big|_{r=\rho} \\
&\quad - \left(\frac{|\partial Y|}{|Z|}\bar{\gamma}_{as} C_e - \bar{\gamma}_{ds}\tilde{S}_{es}\right) \\
&\quad - \frac{|\partial \Gamma|}{|Z|}\left(\frac{\lambda_1 C_e}{1+C_e} - \delta_1\right) \text{ in } (0, l_h), \qquad (3.5a) \\
\left(\theta_b + \frac{|\partial Y|}{|Z|}\frac{\sigma_e}{l}\frac{\gamma_{af}}{\gamma_{df}}\right)\partial_t C_e &= D^b_{eff}\partial_x^2 C_e - \hat{D}\frac{|\partial Y|}{|Z|}\partial_r C_i(t,x,r)\Big|_{r=\rho} \\
&\quad - \left(\frac{|\partial Y|}{|Z|}\bar{\gamma}_{as} C_e - \bar{\gamma}_{ds}\tilde{S}_{es}\right) \text{ in } (l_h, 1) \qquad (3.5b) \\
\partial_t \tilde{S}_{es} &= \frac{|\partial Y|}{|Z|}\bar{\gamma}_{as} C_e - \bar{\gamma}_{ds}\tilde{S}_{es} \text{ in } (0, l_h) \qquad (3.5c) \\
\left(\theta_i + \frac{\sigma_i \zeta_{af}}{\zeta_{df}}\right)\partial_t C_i - \hat{D}\frac{1}{r^2}\partial_r(r^2 \partial_r C_i) &= -(\bar{\zeta}_{as} C_i - \bar{\zeta}_{ds} S_{is}), \text{ in } (0, r_0) \times (0, 1) \qquad (3.5d) \\
\partial_t S_{is} &= \bar{\zeta}_{as} C_i - \bar{\zeta}_{ds} S_{is}, \text{ in } (0, r_0) \times (0, 1), \qquad (3.5e)
\end{aligned}$$

with initial and boundary conditions

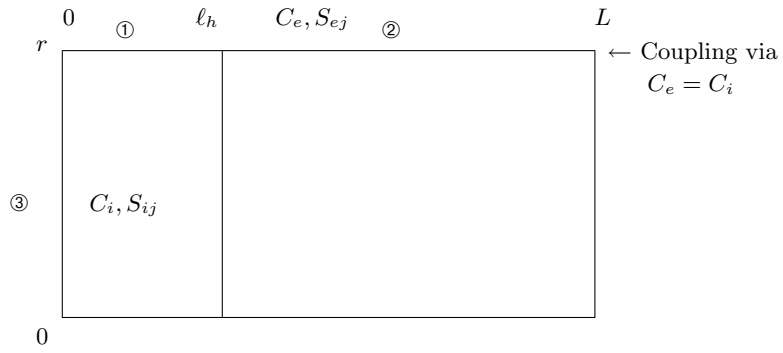

Fig. 3: Simplified domain for solving equations (3.5), where ①,②,③ represent the root hair zone, the zone way from the root hairs, and the intra particle space, respectively.

$$
\begin{aligned}
C_i &= C_e, && \text{on } (0,T)\times\{r=r_0\}\times(0,1),\\
\partial_x C_e &= \frac{\lambda_2 C_e}{k_2 + C_e} - \delta_2, && \text{on } (0,T)\times\{x=0\},\\
\partial_x C_e &= 0, && \text{on } (0,T)\times\{x=1\},\\
C_e(0,x) &= C_{e0}, && \text{in } (0,1),\\
C_i(0,x,r) &= C_{i0} = C_{e0}, && \text{in } (0,r_0)\times(0,1),\\
\tilde{S}_{es}(0,x) &= \tilde{S}_{es0} = \frac{|\partial Y|}{|Z|}\frac{\sigma_e}{l}\frac{\gamma_{as}}{\gamma_{ds}} C_{e0}, && \text{in } (0,l_h),\\
\tilde{S}_{is}(0,x,r) &= \tilde{S}_{is0} = \sigma_i \frac{\zeta_{as}}{\zeta_{ds}} C_{e0}, && \text{in } (0,r_0)\times(0,1),
\end{aligned}
$$

where

$$\tilde{S}_{es} = \frac{1}{|Z|}\int_{\partial Y} S_{es}\, dS,$$

and where $|\partial Y| = |\partial Y_a| = |\partial Y_b|$ is the surface area of the soil particles, which is the same both in and away from the root hair zone and where $|\partial \Gamma|$ is the surface area of the root hairs. Note that the Neumann boundary condition for the macroscale at $x = 1$ implies that the total uptake by the root hair system is equal to the reduction of the total concentration.

4 Numerical Investigations

In this section we numerically investigate our macroscopic model given by equations (3.5). In doing this we need to solve the cell problem in order to

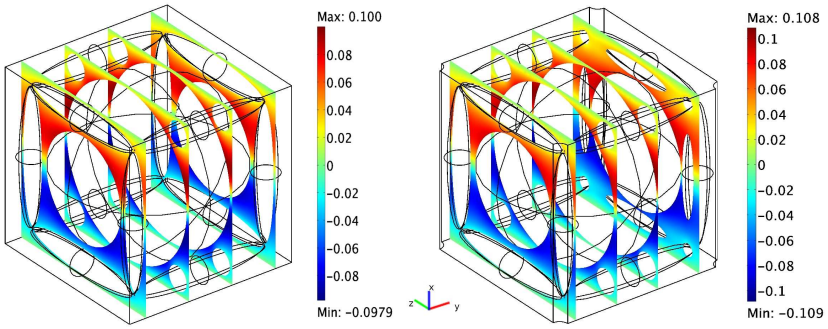

(a) Away from the root hair zone (b) Root hair zone

Fig. 4: Solution of the cell problem, calculated using COMSOL Multiphysics.

calculate the effective diffusion constants D^a_{eff} and D^b_{eff}. We do this in next subsection using COMSOL Multiphysics, where we also discuss the effect of different geometries on the effective diffusivity.

4.1 Numerical solution of the cell problem

In solving the cell problem we consider two different scenarios. More precisely, in the first scenario we assume that the water fraction in the interparticle solution is the same in both zones, which implies that $\theta_a = \theta_b$ and that we have less air in the root hair zone than away from it. In the second scenario, the amount of air in the root hair zone is the same as away from the root hair zone, which implies that $\theta_a < \theta_b$. In Table 4 we present the values of the non-dimensional volume fractions for these two different scenarios as well as the values of the effective diffusion constants D^a_{eff}, D^b_{eff}.

In both scenarios we choose as an effective diffusion constant the value of the xx component of the effective diffusivity matrix, because in our configuration root hairs lie parallel to the x axis. For example, in the case of the second scenario the effective diffusivity matrix away from the root hair zone is given by

$$D_{eff} = \begin{pmatrix} 0.252546 & 5\ 10^{-5} & 4\ 10^{-5} \\ 5\ 10^{-5} & 0.254008 & -9\ 10^{-5} \\ 4\ 10^{-5} & -9\ 10^{-5} & 0.254261 \end{pmatrix},$$

and we choose as $D^b_{eff} = 0.252546$. In Figure 4a we plot the solution of the cell problem away from the root hair zone, while in 4b we plot the solution of the cell problem in the root hair zone for the second scenario.

As we can see in Table 4 the difference in the value of the effective diffusivity for the two different scenarios is very small, so from now on we will conduct our numerical simulations using the values of the parameters

Scenario 1		Scenario 2	
$\|X_a\|$	0.366476	$\|X_a\|$	0.358635
$\|X_b\|$	0.366476	$\|X_b\|$	0.366476
D^a_{eff}	0.249040	D^a_{eff}	0.243551
D^b_{eff}	0.252546	D^b_{eff}	0.252546

Table 4: Volume fractions and effective diffusivities for the two different scenarios

obtained by the second scenario, *i.e.,* when root hairs take up the fluid phase, and the air volume fraction stays the same.

4.2 Results

In this subsection we present the results of numerical simulations. We solve equations (3.5) by using finite differences for the spatial derivatives (details in Appendix B). The resulting ordinary differential equations with respect to time are solved using MATLAB ode15s function. The values of the parameters used for the simulations can be found in Table 5. For the purposes of our numerical simulation we consider two different scenarios related to the uptake properties of the root hairs and the main root. In the first one, the rate constants in the uptake function of the main roots are different than the root hairs ones, while in the second one, the main root and the root hairs have the same uptake properties.

4.2.1 Different uptake properties We start our numerical investigations with the case where the uptake properties of the main root are different from the root hair ones. In particular, we have chosen the values for the main root uptake properties from [13], whilst the values for the root hairs come from [11].

In Figure 5 we plot the concentration in the fluid part for the dual porosity model in the presence and absence of root hairs. As we can see, the concentration in the fluid part in the presence of root hairs is lower than in the absence of root hairs as would be expected, since in the root hair zone, root hairs act like a sink. It is also interesting to notice that in both cases the depletion profiles extend all the way to the boundary of the domain. This indicates that the competition between neighbouring roots starts much quicker than previously thought in experimental context

In Figures 6a,b we plot the rate of nutrient uptake by the main root and root hairs for the dual porosity model as well as the total uptake in the presence and absence of root hairs. In particular, the total uptake rate of the root hairs is given by

$$f_h(t) = \int_0^{l_h} \left(\frac{\lambda_1 C_e(x,t)}{1 + C_e(x,t)} - \delta_1 \right) dx, \tag{4.1}$$

Dimensional parameters		Non Dimensional parameters	
ρ (cm)	$4.99\ 10^{-3}$	r_0	0.499
L (cm)	1	$\hat{D}$	1
l (cm)	10^{-2}	$\bar{\gamma}_{ds} = \bar{\zeta}_{ds}$	0.0026
L_a (cm)	10^{-1}	$\bar{\gamma}_{as}$	0.09
D_l (cm^2 s^{-1})	$9\ 10^{-6}$	$\bar{\zeta}_{as}$	7.55
D_i (cm^2 s^{-1})	$9\ 10^{-10}$	λ_1	1067.63
σ_e (cm^2 cm^{-2})	0.3973	δ_1	46.38
σ_i (cm^2 cm^{-3})	$4\ 10^3$	λ_2^1	62.4521
θ_i (cm^2 cm^{-3})	0.2025	δ_2^1	0.1839
F_h (μmol cm^{-2}s^{-1})	$2.21\ 10^{-7}$	κ_2^1	2.5217
K_h (μmol cm^{-3})	$2.3\ 10^{-3}$	λ_2^2	10.6763
E_h (μmol cm^{-3})	$0.96\ 10^{-8}$	δ_2^1	0.4638
F_r^1 (μmol cm^{-2}s^{-1})	$3.28\ 10^{-6}$	κ_2^2	1
K_r^1 (μmol cm^{-3})	$5.8\ 10^{-3}$	$\lvert\partial\Gamma\rvert$	0.314
E_r^1 (μmol cm^{-3})	$0.96\ 10^{-8}$	$\lvert\partial Y\rvert$	3.129
ρ_h (cm)	10^{-4}	$\frac{\bar{\zeta}_{af}}{\bar{\zeta}_{df}}$	0.1
$[t]$ (sec)	$\frac{10^6}{9}$	$\frac{\bar{\gamma}_{af}}{\bar{\gamma}_{df}}$	0.1
$[C_e]$ (μmol cm^{-3})	$2.3\ 10^{-3}$	l_h	0.1
C_{e0} (μmol cm^{-3})	$2.3\ 10^{-3}$	$\frac{\bar{\gamma}_{af}^1}{\bar{\gamma}_{df}^1}$	483.8318

Table 5: Model parameters used for simulations after [17,2,15,18,11,13].

while the rate of uptake from the root is given by

$$f_r(t) = D_{eff}^a \left(\frac{\lambda_2 C_e(0,t)}{\kappa_2 + C_e(0,t)} - \delta_2 \right). \tag{4.2}$$

The total uptake is calculated as

$$F_{total}(t) = \int_0^t (f_h(s) + f_r(s))ds. \tag{4.3}$$

As we can see the rate of uptake by the root hairs is comparable to the rate of the uptake by the main root; something that indicates that root hairs are very important for the nutrient uptake. This becomes apparent in Figure 6b where we compare the total uptake in the presence and absence of root hairs. In the presence of root hairs, the concentration in the fluid part tends to be smaller than in the absence of root hairs, while the total nutrient uptake after 14 days is roughly 50% more when root hairs are present. This further illustrates the importance of root hairs for the nutrient uptake.

We now plot the same quantities in the case of the single porosity model. For this model we have that $\hat{D} = 0$, which implies that there is no diffusion inside the soil particles and we thus ignore the slow and the fast reactions S_{is}, S_{if}. In order to be able to have a meaningful comparison with the dual porosity model we need to alternate the buffer power $\frac{\bar{\gamma}_{af}}{\bar{\gamma}_{df}}$, in such a way

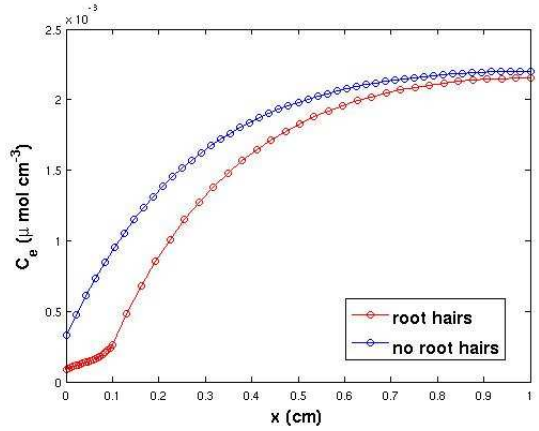

Fig. 5: Concentration in the fluid part at $t = 14$ days, $F_r = 3.28\ 10^{-6}$, μmol cm^{-2}s^{-1} $K_r = 5.8\ 10^{-3}$ μmol cm^{-3}, $E_r = 0.96\ 10^{-8}$ μmol cm^{-3}, $F_h = 2.21\ 10^{-7}$ μmol cm^{-2}s^{-1}, $K_h = 2.3\ 10^{-3}$ μmol cm^{-3}, $E_h = 0.96\ 10^{-8}$ μmol cm^{-3}.

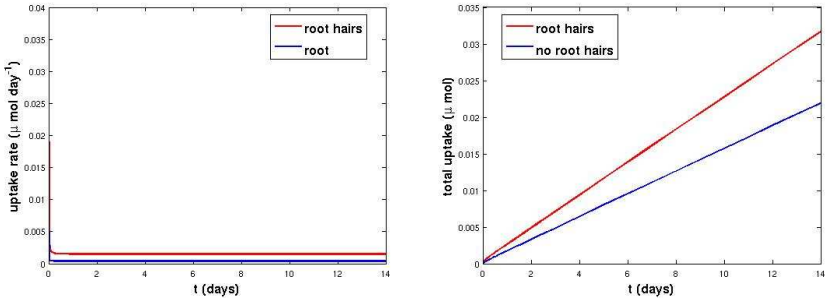

(a) Uptake rate. (b) Total nutrient uptake.

Fig. 6: Root hairs vs no root hairs for the dual porosity model,$F_r = 3.28\ 10^{-6}$, μmol cm^{-2}s^{-1} $K_r = 5.8\ 10^{-3}$ μmol cm^{-3}, $E_r = 0.96\ 10^{-8}$ μmol cm^{-3}, $F_h = 2.21\ 10^{-7}$ μmol cm^{-2}s^{-1}, $K_h = 2.3\ 10^{-3}$ μmol cm^{-3}, $E_h = 0.96\ 10^{-8}$ μmol cm^{-3}.

that total concentration in the soil does not change (see Table 5, $\frac{\bar{\gamma}_{af}^1}{\bar{\gamma}_{df}^1}$), while the same applies for the initial fluid concentration. This has an important effect, since as we can see in Figure 7, the concentration in the fluid part, both for in the presence and absence of roots hairs, now remains higher than in the dual porosity case. This is related to the fact than in the single porosity model the buffer power is higher, which implies that the amount of nutrients bound on the surface of the soil particles is higher than in the dual porosity model. It is also worth mentioning that the depletion profiles now develop only close to the root hair zone and do not extent to the boundary

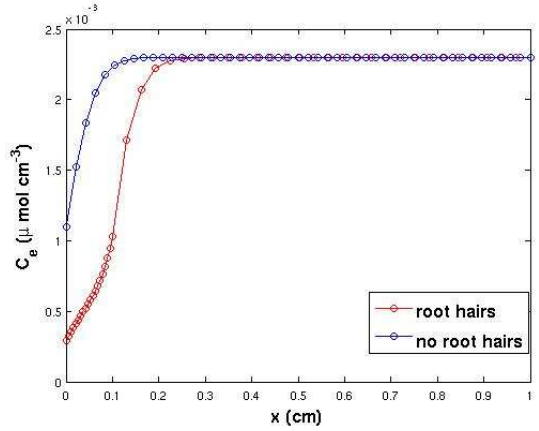

Fig. 7: Concentration in the fluid part at $t = 14$ days,$F_r = 3.28\ 10^{-6}$, μmol cm^{-2}s^{-1} $K_r = 5.8\ 10^{-3}$ μmol cm^{-3}, $E_r = 0.96\ 10^{-8}$ μmol cm^{-3}, $F_h = 2.21\ 10^{-7}$ μmol cm^{-2}s^{-1}, $K_h = 2.3\ 10^{-3}$ μmol cm^{-3}, $E_h = 0.96\ 10^{-8}$ μmol cm^{-3}.

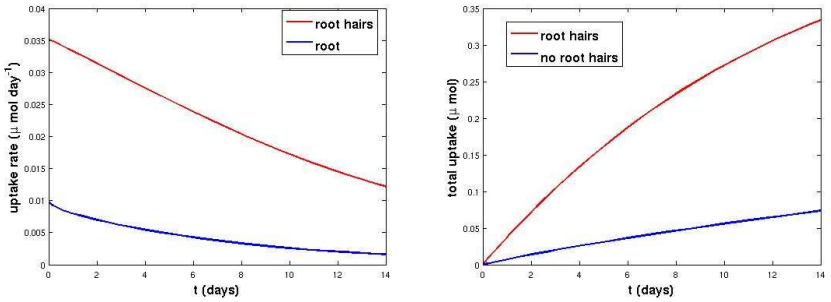

(a) Uptake rate (b) Total nutrient uptake

Fig. 8: Root hairs vs no root hairs for the single porosity model,$F_r = 3.28\ 10^{-6}$, μmol cm^{-2}s^{-1} $K_r = 5.8\ 10^{-3}$ μmol cm^{-3}, $E_r = 0.96\ 10^{-8}$ μmol cm^{-3}, $F_h = 2.21\ 10^{-7}$ μmol cm^{-2}s^{-1}, $K_h = 2.3\ 10^{-3}$ μmol cm^{-3}, $E_h = 0.96\ 10^{-8}$ μmol cm^{-3}.

of our domain, as in the dual porosity case. Consequently, the difference in the total nutrient uptake in the presence and absence of root hairs is even more apparent in the single porosity model as we can see in Figure 8b. This can also be better understood by Figure 8a, where we plot the rate of uptake of nutrients due to root hairs and the main root. As we can see, because of the higher concentration in the fluid part, the uptake rate is now decaying slower as a function of time in comparison with the dual porosity case and it is also larger in magnitude.

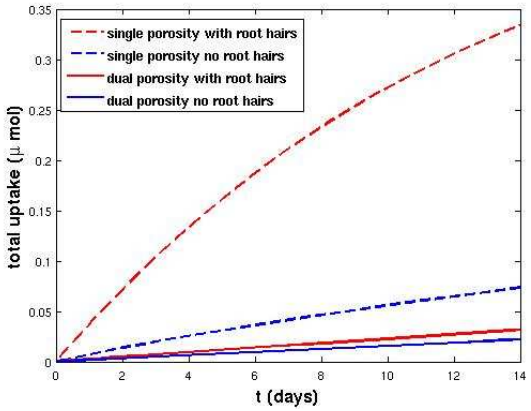

Fig. 9: Comparison of the total nutrient uptake between the dual and the single porosity models, $F_r = 3.28\ 10^{-6}$, μmol cm^{-2}s^{-1} $K_r = 5.8\ 10^{-3}$ μmol cm^{-3}, $E_r = 0.96\ 10^{-8}$ μmol cm^{-3}, $F_h = 2.21\ 10^{-7}$ μmol cm^{-2}s^{-1}, $K_h = 2.3\ 10^{-3}$ μmol cm^{-3}, $E_h = 0.96\ 10^{-8}$ μmol cm^{-3}.

Finally, in Figure 9 we plot the total nutrient uptake as a function of time in the presence and absence of the root hairs both for the single and dual porosity models. The total nutrient uptake is higher than the dual porosity case, both in the presence and in the absence of root hairs. However, this should not be a surprise, since as we have already mentioned in the single porosity case, the buffer power is greater than in the dual porosity one, which results in higher concentrations in the fluid part and thus higher total nutrient uptake.

4.2.2 Same uptake properties We now study the case where the uptake properties of the main root are the same with the root hairs ones. In particular, we have chosen our root and root hair uptake property values from [11]. We start our investigations in a similar way as before by plotting the concentration in the fluid part (Figure 10). The picture is similar to the one in Figure 5, with the fluid concentration in the presence of hairs to be lower than in the absence of hairs.

We now compare the uptake rates in Figure 11a due to the root hairs and the main root and we obtain a similar picture to Figure 6a, with the rate of uptake due to the root hairs being higher than the uptake by the main root. However, when we compare the total nutrient uptake in the presence and absence of root hairs (Figure 11b), we see that for this set of parameters the presence of root hairs is even more important for the total nutrient uptake than before. In particular, we see that the total nutrient uptake in the presence of root hairs is now roughly 100% more than in the absence of root hairs. This is to be expected, since for this particular choice of parameters the root has smaller uptake properties than before.

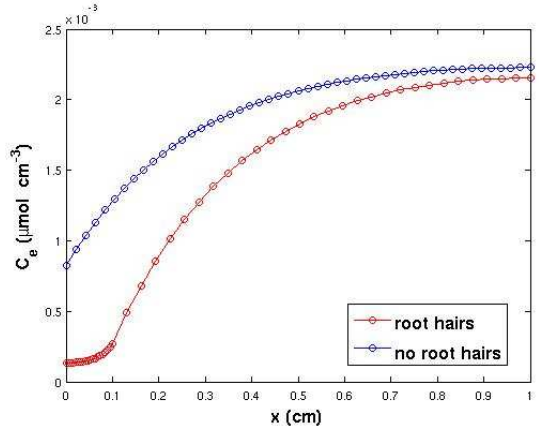

Fig. 10: Concentration in the fluid part at $t = 14$ days, $F_r = F_h = 2.21\ 10^{-7}$ μmol cm^{-2}s^{-1}, $K_r = K_h = 2.3\ 10^{-3}$ μmol cm^{-3}, $E_r = E_h = 0.96\ 10^{-8}$ μmol cm^{-3}.

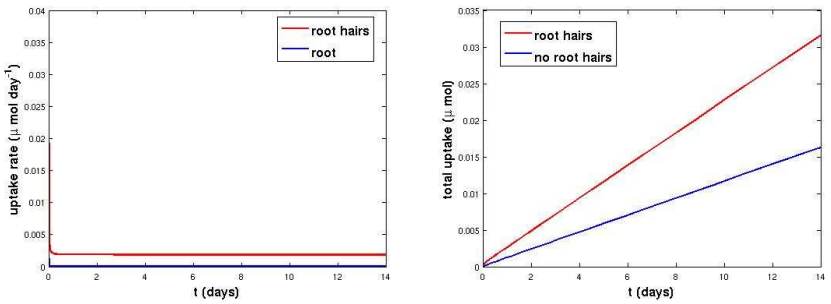

(a) Uptake rate (b) Total nutrient uptake

Fig. 11: Root hairs vs no root hairs for the dual porosity model, $F_r = F_h = 2.21\ 10^{-7}$ μmol cm^{-2}s^{-1}, $K_r = K_h = 2.3\ 10^{-3}$ μmol cm^{-3}, $E_r = E_h = 0.96\ 10^{-8}$ μmol cm^{-3}.

We now proceed to studying the same quantities for the single porosity model. Again we have changed the buffer power in order for the total nutrient amount in the soil and the initial fluid concentration to be the same with the dual porosity case. As we can see in Figure 12, the concentration in the fluid part in the presence of root hairs is lower than in the absence of root hairs, while again the main concentration gradients are close to the main root and the root hair zone.

In Figures 13a,b we plot the uptake rate by the root hairs and the main root as well as the total nutrient uptake in the presence and absence of root hairs. The rate of uptake due to the root hairs is greater than the one in Figure 8a, which again relates to the fact that the uptake properties of the

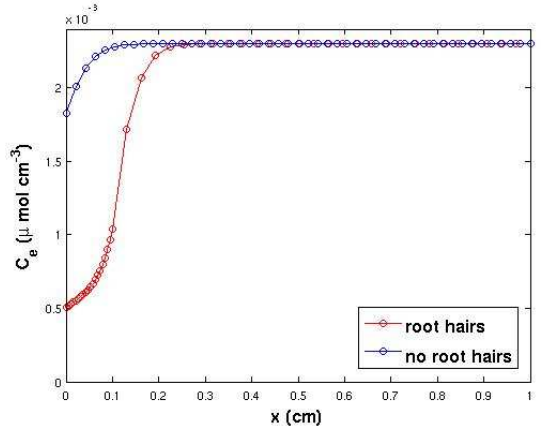

Fig. 12: Concentration in the fluid part at $t = 14$ days, $F_r = F_h = 2.21\ 10^{-7}$ μmol cm^{-2}s^{-1}, $K_r = K_h = 2.3\ 10^{-3}$ μmol cm^{-3}, $E_r = E_h = 0.96\ 10^{-8}$ μmol cm^{-3}.

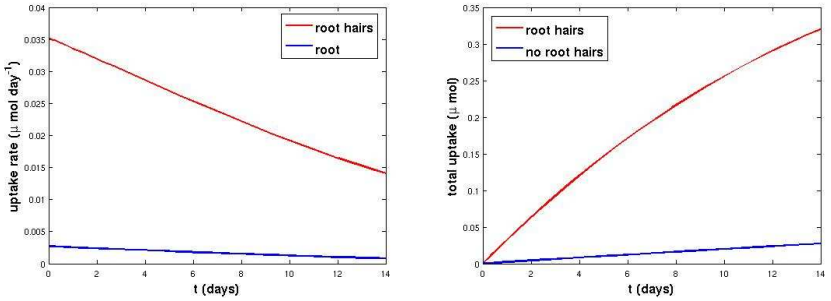

(a) Uptake rate (b) Total nutrient uptake

Fig. 13: Root hairs vs no root hairs for the single porosity model, $F_r = F_h = 2.21\ 10^{-7}$ μmol cm^{-2}s^{-1}, $K_r = K_h = 2.3\ 10^{-3}$ μmol cm^{-3}, $E_r = E_h = 0.96\ 10^{-8}$ μmol cm^{-3}.

main root for this set of parameters are smaller than before. This becomes more apparent in Figure 14, where we compare the total nutrient uptake for the dual and single porosity models in the presence and absence of root hairs. As we can clearly see, for this set of parameters the presence of root hairs is more important than before for the total nutrient uptake both for the single, but also for the dual porosity model.

5 Conclusions

Using a detailed microscopic description, we have derived a macroscopic dual porosity model for the uptake of nutrients by root hairs. These macro-

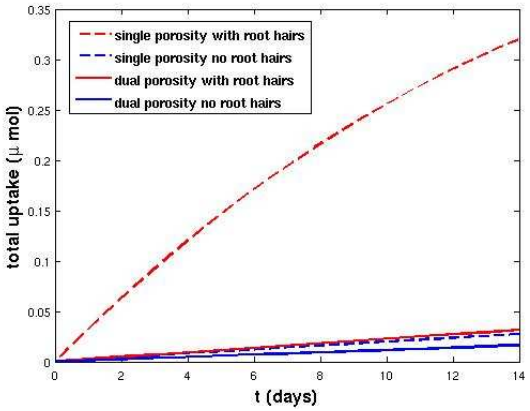

Fig. 14: Comparison of the total uptake between the dual and the single porosity models, $F_r = F_h = 2.21\ 10^{-7}$ μmol cm^{-2}s^{-1}, $K_r = K_h = 2.3\ 10^{-3}$ μmol cm^{-3}, $E_r = E_h = 0.96\ 10^{-8}$ μmol cm^{-3}.

scopic equations depend on the geometric properties of the microscale as well as on the uptake properties of the root hairs. A simplified model with one macroscopic and one microscopic dimension was then considered and studied numerically for different root uptake properties and compared with a single porosity model. In all cases, the presence of root hairs increased the total nutrient uptake, while the relative increase was depended on the uptake properties of the main root. This effect is even more profound in the single porosity case, since then the nutrients can only bound on the particle surface which leads to higher concentrations in the fluid part and thus higher total nutrient uptake.

Acknowledgements

K. C. Zygalakis was supported by Award No. KUK-C1-013-04, made by the King Abdullah University of Science and Technology (KAUST). T. Roose is a Royal Society University Research Fellow. We would like to thank Ian Griffiths, Nick Hale, James Lottes, Guy Kirk and Matthias Wissuwa for various discussions regarding this manuscript.

References

1. Vaccari, D. A. (June 2009) Phosphorus Famine: The Threat to Our Food Supply, *Scientific American*.
2. Tinker, P. B. and Nye, P. H. (2000) Solute movement in the rhizosphere, Oxford Univ. Press, New York, Oxford.
3. Marschner, H. (1995) Mineral nutrition of higher plants, London UK: Academic Press.

4. Narang, R., Bruene, A., and Altmann, T. (2000) Anaysis of phospate acquisition efficiency in different Arabidopsis accessions, *Plant Physiology* **124**, 1786–1799.
5. Wissuwa, M. (2003) How do plants achieve tolerance to phosphorus deficiency? Small casuses with big effects, *Plant Physiology* **133**, 1947–1958.
6. Passioura, J. (1963) A mathematical model for the uptake of ions from the soil solution, *Plant and Soil* **18**, 225–238.
7. Bhat, K. K. S., Nye, P., and Baldwin, J. P. (1976) Diffusion of phospate to plant roots in soil IV. The concentration distance profile in the rhizosphere of root hairs in a low P-soil, *Plant and Soil* **44**, 63–72.
8. Geelhoed, J. S., Mous, S. L. J., and Findenegg, G. R. (1997) Modelling zero sink nutrient uptake by roots with root hairs from soil: Comparison of two models, *Soil Science* **162**, 544–553.
9. Hornung, U. (1997) Homogenization and Porous Media, Springer-Verlag, New York.
10. Pavliotis, G. and Stuart, A. (2008) Multiscale Methods: Averaging and Homogenization, Springer-Verlag, New York.
11. Leitner, D., Klepsch, S., Ptashnyk, M., Marchant, A., Kirk, G. J. D., Schnepf, A., and Roose, T. (Feb 2010) A dynamic model of nutrient uptake by root hairs, *New Phytologist* **185(3)**, 792–802.
12. Ptashnyk, M., Roose, T., and Kirk, G. J. D. (Feb 2010) Diffusion of strongly sorbed solutes in soil: a dual-porosity model allowing for slow access to sorption sites and time-dependent sorption reactions, *European Journal of Soil Science* **61(1)**, 108–119.
13. Ptashnyk, M. and Roose, T. (in press) Derivation of macroscopic model for transport of strongly sorbed solutes in the soil using homogenization techniques, *SIAM J. Appl. Math.*
14. Barber, S. A. (1984) Soil Nutrient Bioavailability. A Mechanistic Approach., A Wiley-Interscience Publication, New York.
15. Nye, P. H. and Staunton, S. (1994) The self-diffusion of strongly adsorbed anions in soil: two path model to simulate restricted access to exchange sites, *European Journal of Soil Science* **45**, 145–152.
16. Roose, T. and Kirk, G. J. D. (2009) The solution of convection-diffusion equations for solute transport to plant roots, *Plant and Soil* **316**, 1–2.
17. Roose, T. (2000) Mathematical model of plant nutrient uptake, PhD thesis University of Oxford.
18. Roose, T., Fowler, A. C., and Darrah, P. R. (2001) A mathematical model of plant nutrient uptake, *J. Math. Biol* **42**, 347–360.
19. Morton, K. W. and Mayers, D. F. (2005) Numerical solution of partial differential equations. An introduction, Cambridge University Press, Cambridge second edition.

Appendix A: Homogenization and derivation of macro-scale models using multiple scale asymptotic expansion

By re-scaling Equation (2.8) we obtain the following model

$$\frac{\partial C_e}{\partial t} = \nabla_x^2 C_e, \text{ in } X_a^\epsilon \cup X_b^\epsilon \tag{A.1a}$$

$$\frac{\partial \theta_i C_i}{\partial t} = \epsilon^2 \hat{D} \nabla_x^2 C_i - \frac{\partial S_{i1}}{\partial t} - \frac{\partial S_{i2}}{\partial t}, \text{ in } Y_a^\epsilon \cup Y_b^\epsilon \tag{A.1b}$$

$$\nabla_x C_e \cdot \nu = \epsilon^2 \hat{D} \nabla_x C_i \cdot \nu - \epsilon \frac{\partial S_{e1}}{\partial t} - \epsilon \frac{\partial S_{e2}}{\partial t}, \text{ on } \partial Y_a^\epsilon \cup \partial Y_b^\epsilon, \tag{A.1c}$$

$$C_e = C_i, \text{ on } \partial Y_a^\epsilon \cup \partial Y_b^\epsilon, \tag{A.1d}$$

$$\nabla_x C_e \cdot \nu = 0, \text{ on } \partial \bar{Y}_a^\epsilon \cup \partial \bar{Y}_b^\epsilon, \tag{A.1e}$$

$$-\nabla_x C_e \cdot \nu = \epsilon F_1, \text{ on } \partial \Gamma_a^\epsilon, \tag{A.1f}$$

where $\hat{D} = D_i/(D_l \epsilon^2) \sim \mathcal{O}(1)$. Equation (A.1) is defined in a complicated space domain consisting of many individual soil particles and root hairs. For the final model we need equations for average concentrations defined in a simpler domain. We do this using homogenization theory. We also split our domain in two parts, far away from the root hair zone and in the hair zone, deriving two sets of effective equations, depending on which domain we are in. In terms of parameters the most interesting regime is the one where $\hat{D} = \mathcal{O}(1)$ and the root hairs contribution is comparable to the main root contribution, *i.e.,* $F_1 \sim \mathcal{O}(1)$. It is also the most relevant experimentally and it is thus the regime we study.

Equations away from the root hair zone

To derive the macroscopic equations we use the following asymptotic expansion with respect to ϵ:

$$\begin{aligned} C_e &= C_e^0 + \epsilon C_e^1 + \epsilon^2 C_e^2 + \cdots, \\ C_i &= C_i^0 + \epsilon C_i^1 + \epsilon^2 C_i^2 + \cdots, \\ S_{en} &= S_{en}^0 + \epsilon S_{en}^1 + \epsilon^2 S_{en}^2 + \cdots, \\ S_{in} &= S_{in}^0 + \epsilon S_{in}^1 + \epsilon^2 S_{in}^2 + \cdots, \end{aligned}$$

for $n = s, f$ for the fast and slow reactions, to obtain (for the equations in the domain)

$$\mathcal{O}(\epsilon^{-2}) \quad \nabla_y^2 C_e^0 = 0, \tag{A.2a}$$

$$\mathcal{O}(\epsilon^{-1}) \quad \nabla_y^2 C_e^1 = -\nabla_x \cdot \nabla_y C_e^0 - \nabla_y \cdot \nabla_x C_e^0, \tag{A.2b}$$

$$\mathcal{O}(1) \quad \nabla_y^2 C_e^2 = \frac{\partial C_e^0}{\partial t} - \nabla_x \cdot \nabla_y C_e^1 - \nabla_y \cdot \nabla_x C_e^1 - \nabla_x^2 C_e^0, \tag{A.2c}$$

$$\mathcal{O}(1) \quad \hat{D} \nabla_y^2 C_i^0 = -\frac{\theta_i \partial C_i^0}{\partial t} + \frac{\partial S_{is}^0}{\partial t} + \frac{\partial S_{if}^0}{\partial t}, \tag{A.2d}$$

$$\mathcal{O}(1) \quad C_e^0 = C_i^0. \tag{A.2e}$$

The boundary condition reads (up to terms of order 1)

$$\left(\frac{1}{\epsilon^2}\nabla_y C_e^0 + \frac{1}{\epsilon}\nabla_y C_e^1 + \nabla_y C_e^2 + \frac{1}{\epsilon}\nabla_x C_e^0 + \nabla_x C_e^1\right)\cdot\nu = \hat{D}\nabla_y C_i^0\cdot\nu - \frac{\partial S_{e1}}{\partial t} - \frac{\partial S_{e2}}{\partial t}, \text{ on } \partial Y_b,$$

and

$$\frac{1}{\epsilon^2}\nabla_y C_e^0\cdot\nu + \frac{1}{\epsilon}\left(\nabla_y C_e^1\cdot\nu + \nabla_x C_e^0\cdot\nu\right) + \left(\nabla_y C_e^2\cdot\nu + \nabla_x C_e^1\cdot\nu\right) = 0 \text{ on } \partial\bar{Y}_b.$$

Equation (A.2a) implies that C_e^0 is a function of x only. Using this and the boundary condition the $\mathcal{O}(\epsilon^{-1})$ equations read

$$\begin{aligned}\nabla_y^2 C_e^1 &= -\nabla_y\cdot(\nabla_x C_e^0),\\ \nabla_y C_e^1\cdot\nu &= -\nabla_x C_e^0\cdot\nu.\end{aligned}$$

This set of equations implies that $C_e^1(x,y) = \chi(y)\cdot\nabla_x C_e^0$ and using this anzatz we obtain the cell problem

$$\nabla_y\cdot\nabla_y\chi = 0, \text{ on } X_b, \tag{A.3a}$$

$$(\nabla_y\chi + I)\cdot\nu = 0, \text{ on } \partial Y_b\cup\partial\bar{Y}_b. \tag{A.3b}$$

The $\mathcal{O}(1)$ equations read

$$\begin{aligned}\nabla_y^2 C_e^2 &= \frac{\partial C_e^0}{\partial t} - \nabla_x\cdot\nabla_y C_e^1 - \nabla_y\cdot\nabla_x C_e^1 - \nabla_x^2 C_e^0,\\ \left(\nabla_y C_e^2 + \nabla_x C_e^1\right)\cdot\nu &= \hat{D}\nabla_y C_i^0\cdot\nu - \frac{\partial S_{es}^0}{\partial t} - \frac{\partial S_{ef}^0}{\partial t},\\ \left(\nabla_y C_e^2 + \nabla_x C_e^1\right)\cdot\nu &= 0,\\ \frac{\partial(\theta_i C_i^0)}{\partial t} &= \hat{D}\nabla_y^2 C_i^0 - \frac{\partial S_{is}^0}{\partial t} - \frac{\partial S_{if}^0}{\partial t}.\end{aligned}$$

We now average the equation for C_e^2 over the unit cell to obtain

$$\int_{X_b}\nabla_y\cdot\nabla_y C_e^2 dy = \int_{X_b}\left(\frac{\partial C_e^0}{\partial t} - \nabla_x\cdot\nabla_y C_e^1 - \nabla_y\cdot\nabla_x C_e^1 - \nabla_x^2 C_e^0\right)dy,$$

and using the specific form of C_e^1, together with the fact that C_e^0 is a function of x only we obtain

$$\int_{X_b}\nabla_y\cdot\nabla_y C_e^2 dy = |X_b|\frac{\partial C_e^0}{\partial t} - \nabla_x\cdot\left[\int_{X_b}((\nabla_y\chi)^T + I)dy\right]\nabla_x C_e^0 - \int_{X_b}\nabla_y\cdot\nabla_x C_e^1 dy, \tag{A.4}$$

By using the divergence theorem the left hand side of (A.4) becomes

$$\begin{aligned}\int_{X_b}\nabla_y\cdot\nabla_y C_e^2 dy &= \int_{\partial Y_b}\nabla_y C_e^2\cdot\nu ds + \int_{\partial\bar{Y}_b}\nabla_y C_e^2\cdot\nu ds,\\ &= \int_{\partial Y_b}\hat{D}\nabla_y C_i^0\cdot\nu ds - \int_{\partial Y_b\cup\partial\bar{Y}_b}\nabla_x C_e^1\cdot\nu dS - \int_{\partial Y_b}\left(\frac{\partial S_{es}^0}{\partial t} + \frac{\partial S_{ef}^0}{\partial t}\right)dS,\\ &= \int_{\partial Y_b}\hat{D}\nabla_y C_i^0\cdot\nu dS - \int_{X_b}\nabla_y\cdot\nabla_x C_e^1 dy - \int_{\partial Y_b}\left(\frac{\partial S_{es}^0}{\partial t} + \frac{\partial S_{ef}^0}{\partial t}\right)dS.\end{aligned}$$

Thus we obtain the effective set of equations

$$|X_b|\frac{\partial C_e^0}{\partial t} = \nabla_x \cdot \left[\int_{X_b} ((\nabla_y \chi)^T + I)dy\right] \nabla_x C_e^0 + \int_{\partial Y_b} \hat{D}\nabla_y C_i^0 \cdot \nu dS - \int_{\partial Y_b} \left(\frac{\partial S_{es}^0}{\partial t} + \frac{\partial S_{ef}^0}{\partial t}\right) dS,$$
$$\theta_i \frac{\partial C_i^0}{\partial t} = \hat{D}\nabla_y^2 C_i^0 - \frac{\partial S_{is}^0}{\partial t} - \frac{\partial S_{if}^0}{\partial t},$$
$$C_e = C_i.$$

Equations in the root hair zone

To derive the macroscopic equations we use the following asymptotic expansion with respect to ϵ:

$$\begin{aligned} C_e &= C_e^0 + \epsilon C_e^1 + \epsilon^2 C_e^2 + \cdots, \\ C_i &= C_i^0 + \epsilon C_i^1 + \epsilon^2 C_i^2 + \cdots, \\ S_{en} &= S_{en}^0 + \epsilon S_{en}^1 + \epsilon^2 S_{en}^2 + \cdots, \\ S_{in} &= S_{in}^0 + \epsilon S_{in}^1 + \epsilon^2 S_{in}^2 + \cdots, \\ F_1 &= f_0 + \epsilon f_1 + \epsilon^2 f_2 + \cdots, \end{aligned}$$

for $n = s, f$ for the fast and slow reactions, to obtain (for the equations in the domain)

$$\mathcal{O}(\epsilon^{-2})\ \nabla_y^2 C_e^0 = 0, \tag{A.5a}$$
$$\mathcal{O}(\epsilon^{-1})\ \nabla_y^2 C_e^1 = -\nabla_x \cdot \nabla_y C_e^0 - \nabla_y \cdot \nabla_x C_e^0, \tag{A.5b}$$
$$\mathcal{O}(1)\ \ \nabla_y^2 C_e^2 = \frac{\partial C_e^0}{\partial t} - \nabla_x \cdot \nabla_y C_e^1 - \nabla_y \cdot \nabla_x C_e^1 - \nabla_x^2 C_e^0, \tag{A.5c}$$
$$\mathcal{O}(1)\ \ \nabla_y^2 C_i^0 = -\frac{\theta_i \partial C_i^0}{\partial t} + \frac{\partial S_{is}^0}{\partial t} + \frac{\partial S_{if}^0}{\partial t}, \tag{A.5d}$$
$$\mathcal{O}(1)\ \ C_e^0 = C_i^0. \tag{A.5e}$$

The boundary condition reads (up to terms of order 1)

$$\left(\frac{1}{\epsilon^2}\nabla_y C_e^0 + \frac{1}{\epsilon}\nabla_y C_e^1 + \nabla_y C_e^2 + \frac{1}{\epsilon}\nabla_x C_e^0 + \nabla_x C_e^1\right)\cdot\nu = \hat{D}\nabla_y C_i^0 \cdot \nu - \frac{\partial S_{e1}}{\partial t} - \frac{\partial S_{e2}}{\partial t}, \text{ on } \partial Y_a,$$

and

$$\frac{1}{\epsilon^2}\nabla_y C_e^0 \cdot \nu + \frac{1}{\epsilon}\left(\nabla_y C_e^1 \cdot \nu + \nabla_x C_e^0 \cdot \nu\right) + \left(\nabla_y C_e^2 \cdot \nu + \nabla_x C_e^1 \cdot \nu\right) = 0, \text{ on } \partial \bar{Y}_a,$$

and

$$\frac{1}{\epsilon^2}\nabla_y C_e^0 \cdot \nu + \frac{1}{\epsilon}\left(\nabla_y C_e^1 \cdot \nu + \nabla_x C_e^0 \cdot \nu\right) + \left(\nabla_y C_e^2 \cdot \nu + \nabla_x C_e^1 \cdot \nu\right) = -f_0, \text{ on} \partial \Gamma_a.$$

Equation (A.5a) implies that C_e^0 is a function of x only. Using this and the boundary condition the $\mathcal{O}(\epsilon^{-1})$ equations read

$$\begin{aligned}\nabla_y^2 C_e^1 &= -\nabla_y \cdot (\nabla_x C_e^0),\\ \nabla_y C_e^1 \cdot \nu &= -\nabla_x C_e^0 \cdot \nu.\end{aligned}$$

This set of equation implies that $C_e^1(x,y) = \chi(y) \cdot \nabla_x C_e^0$ and using this anzatz we obtain the cell problem

$$\nabla_y \cdot \nabla_y \chi = 0, \text{ on } X_a, \tag{A.6a}$$

$$(\nabla_y \chi + I) \cdot \nu = 0, \text{ on } \partial Y_a \cup \partial \bar{Y}_a \cup \partial \Gamma_a. \tag{A.6b}$$

The $\mathcal{O}(1)$ equations read

$$\begin{aligned}\nabla_y^2 C_e^2 &= \frac{\partial C_e^0}{\partial t} - \nabla_x \cdot \nabla_y C_e^1 - \nabla_y \cdot \nabla_x C_e^1 - \nabla_x^2 C_e^0,\\ \left(\nabla_y C_e^2 + \nabla_x C_e^1\right) \cdot \nu &= \hat{D} \nabla_y C_i^0 \cdot \nu - \frac{\partial S_{es}^0}{\partial t} - \frac{\partial S_{ef}^0}{\partial t},\\ \left(\nabla_y C_e^2 + \nabla_x C_e^1\right) \cdot \nu &= 0,\\ \left(\nabla_y C_e^2 + \nabla_x C_e^1\right) \cdot \nu &= -f_0,\\ \frac{\partial(\theta_i C_i^0)}{\partial t} &= \nabla_y^2 C_i^0 - \frac{\partial S_{is}^0}{\partial t} - \frac{\partial S_{if}^0}{\partial t}.\end{aligned}$$

So if we now average over the unit cell X_a, we obtain the following effective equation:

$$\begin{aligned}|X_a| \frac{\partial C_e^0}{\partial t} &= \nabla_x \cdot \left[\int_{X_a} ((\nabla_y \chi)^T + I) dy\right] \nabla_x C_e^0 + \int_{\partial Y_a} \hat{D} \nabla_y C_i^0 \cdot \nu dS\\ &\quad - \int_{\partial \Gamma} f_0 dS - \int_{\partial Y_a} \left(\frac{\partial S_{es}^0}{\partial t} + \frac{\partial S_{ef}^0}{\partial t}\right) dS,\\ \theta_i \frac{\partial C_i^0}{\partial t} &= \nabla_y^2 C_i^0 - \frac{\partial S_{is}^0}{\partial t} - \frac{\partial S_{if}^0}{\partial t},\\ C_e &= C_i.\end{aligned}$$

where the solution to the cell problem χ satisfies

$$\nabla_y \cdot \nabla_y \chi = 0, \text{ on } X_a, \tag{A.7a}$$

$$(\nabla_y \chi + I) \cdot \nu = 0, \text{ on } \partial Y_a \cup \partial \bar{Y}_a \cup \partial \Gamma. \tag{A.7b}$$

Expansion of Michaelis Menten flux

We now derive the term f_0 appearing in the homogenized equation in the root hair zone. Remember that the Michaelis Menten flux for the uptake by root hairs is given by

$$F_1 = \frac{\lambda_1 C_e}{1 + C_e} - \delta_1.$$

Substituting the expansion of powers of ϵ for C_e we obtain:

$$\begin{aligned}\frac{1}{1+C_e} &= \frac{1}{1+C_e^0}\frac{1}{1+\epsilon\frac{1}{1+C_e^0}(C_e^1+\epsilon C_e^2)},\\ &= \frac{1}{1+C_e^0}\left(1-\epsilon\frac{C_e^1}{1+C_e^0}+\epsilon^2\left[\frac{(C_e^1)^2}{(1+C_e^0)^2}-\frac{C_e^2}{1+C_e^0}\right]-\mathcal{O}(\epsilon^3)\right).\end{aligned}$$

This implies that F_1 can be expanded in powers of ϵ as

$$F_1 = f_0 + \epsilon f_1 + \epsilon^2 f_2,$$

with

$$\begin{aligned}f_0 &= \lambda_1\frac{C_e^0}{1+C_e^0}-\delta_1,\\ f_1 &= \lambda_1\left(\frac{C_e^1}{1+C_e^0}-\frac{(C_e^1)^2C_e^0}{(1+C_e^0)^2}\right),\\ f_2 &= \lambda_1\left(\frac{C_e^2}{(1+C_e^0)}-\frac{(C_e^1)^2+C_e^0C_e^2}{(1+C_e^0)^2}+\frac{C_e^0(C_e^1)^2}{(1+C_e^0)^3}\right).\end{aligned}$$

Appendix B: Numerical solution of (3.5)

Equations (3.5) are solved using a finite difference approximation for the space derivatives. The second order partial derivative of C_e with respect to x was discretized using a second order central difference in each of the two domains (root hair zone and away from the root hair zone). On the internal boundary $x = l_h$ we need to account for the continuity of C_e and its derivative as well as the fact that the space-step used in the root hair zone is in principle different than the one used away from the root hair zone. We thus approximate the second spatial derivative of C_e on the internal boundary $x = l_h$ in the following way

$$\begin{aligned}\delta_x^2 C(l_h) = &\frac{2D_{eff}^a}{\Delta x(\Delta x+\Delta y)}C(l_h-\Delta x)-\frac{2}{\Delta x+\Delta y}\left(\frac{D_{eff}^a}{\Delta x}+\frac{D_{eff}^b}{\Delta y}\right)C(l_h)\\ &+\frac{2D_{eff}^b}{\Delta y(\Delta x+\Delta y)}C(l_h+\Delta y),\end{aligned}$$

where Δx is the space-step used in the root hair zone and Δy is the space-step used away from the root hair zone. The second order partial derivative of C_i is calculated using a central difference scheme that takes into account the radial symmetry of the problem [19].

RECENT REPORTS

30/09	An hp-Local Discontinuous Galerkin method for Parabolic Integro-Differential Equations	Pani Yadav
31/09	Stochastic neural field theory and the system-size expansion	Bressloff
32/09	A Hamiltonian Krylov-Schur-type method based on the symplectic Lanczos process	Benner Faßbender Stoll
33/09	Nematic liquid crystals : from Maier-Saupe to a continuum theory	Ball Majumdar
34/09	Tangent unit-vector fields: nonabelian homotopy invariants and the Dirichlet energy	Majumdar Robbins Zyskin
35/09	A metabolite-sensitive, thermodynamically-constrained model of cardiac cross-bridge cycling: Implications for force development during ischemia	Tran Smith Loiselle Crampin
36/09	Modelling bacterial behaviour close to a no-slip plane boundary: the influence of bacterial geometry	Shum Gaffney Smith
37/09	Optimal L2-error estimates for the semidiscrete Galerkin approximation to a second order linear parabolic initial and boundary value problem with nonsmooth initial data	Goswami Pani
38/09	Optimal L2 estimates for semidiscrete Galerkin methods for parabolic integro-differential equations with nonsmooth data	Goswami Pani Yadav
39/09	Spatially structured oscillations in a two-dimensional excitatory neuronal network with synaptic depression	Kilpatrick Bressloff
40/09	Stationary bumps in a piecewise smooth neural field model with synaptic depression	Kilpatrick Bressloff
41/09	Homogenization for advection-diffusion in a perforated domain	Haynes Hoang Norris Zygalakis
42/09	Fast stochastic simulation of biochemical reaction systems by alternative formulations of the Chemical Langevin Equation	Melykuti Burrage Zygalakis
43/09	Pseudoreplication invalidates the results of many neuroscientific studies	Lazic

44/09	Cardiac cell modelling: Observations from the heart of the cardiac physiome project	Finka *et al.*
45/09	A Hybrid Radial Basis Function - Pseudospectral Method for Thermal Convection in a 3-D Spherical Shell	Wright Flyer
46/09	Refining self-propelled particle models for collective behaviour	Yates Baker Erban Maini
47/09	Stochastic Partial Differential Equations as priors in ensemble methods for solving inverse problems	Potsepaev Farmer Aziz
48/09	DifFUZZY: A fuzzy spectral clustering algorithm for complex data sets	Cominetti *et al.*
01/10	Fluctuations and instability in sedimentation	Guazzelli Hinch
02/10	Determining the equation of state of highly plasticised metals from boundary velocimetry	Hinch
03/10	Stability of bumps in piecewise smooth neural elds with nonlinear adaptation	Kilpatrick Bressloff
04/10	Random intermittent search and the tug–of–war model of motor–driven transport	Newby Bressloff
05/10	Ergodic directional switching in mobile insect groups	Escudero *et al.*

Copies of these, and any other OCCAM reports can be obtained from:

Oxford Centre for Collaborative Applied Mathematics
Mathematical Institute
24 - 29 St Giles'
Oxford
OX1 3LB
England
www.maths.ox.ac.uk/occam